Terahertz near-field spectroscopy of filled subwavelength sized apertures in thin metal films

J. R. Knab,[1,2] **A. J. L. Adam,**[1] **E. Shaner,**[3] **H. J. A. J. Starmans,**[1] **and P. C. M. Planken**[1,*]

[1] *Department of Imaging Science and Technology, Faculty of Applied Sciences, Delft University of Technology, Lorentzweg 1, 2628 CJ Delft, The Netherlands*

[2] *Current Address: Department of Physics, University of Maryland, Baltimore County, 1000 Hilltop Circle, Baltimore, MD 21250, USA*

[3] *Sandia National Laboratories, Albuquerque, New Mexico 87185 USA*

[*] *p.c.m.planken@tudelft.nl*

Abstract: We have measured terahertz near-field spectra of cesium iodide crystals as small as $\sim$10 μm in diameter, which were deposited on single, sub-wavelength-sized apertures created in thin gold films on a substrate. The advantage of using small apertures for terahertz microspectroscopy is that only terahertz light that has interacted with the cesium iodide is observed. We find that around the transverse optical phonon frequency of cesium iodide, the amplitude transmission is as much influenced by the refractive index as by the absorption. We show that the ability to measure in the near-field of the apertures, where signals are relatively strong, allows us to measure on sample volumes as small as $\sim 5\times10^{-16}$ m^3.

OCIS codes: (180.4243) Near-field microscopy;(300.6495) Spectroscopy, terahertz;(170.6795) Terahertz imaging.

References and links

1. P. U. Jepsen and B. M. Fisher, "Dynamic range in terahertz time-domain transmission and reflection spectroscopy," Opt. Lett. **30**, 29–31 (2005).
2. M. Walther, B. Fischer, and P. U. Jepsen, "Noncovalent intermolecular forces in polycrystalline and amorphous saccharides in the far infrared," Chem. Phys. **288**, 261-268 (2003).
3. Y. C. Shen, P. C. Upadhya, E. H. Linfield, and A. G. Davies, "Temperature-dependent low-frequency vibrational spectra of purine and adenine," Appl. Phys. Lett. **82**, 2350–2352 (2003).
4. M. B. Johnston, L. M. Herz, A. Khan, A. Köhler, A. G. Davies, and E. H. Linfield, "Low-energy vibrational modes in phenylene oligomers studied by THz time-domain spectroscopy," Chem. Phys. Lett. **377**, 256262 (2003).
5. R. Chakkittakandy, J. A. W. M. Corver, and P. C. M. Planken, "Terahertz spectroscopy to identify the polymorphs in freeze-dried mannitol," J. Pharm. Sci. **99**, 932–940 (2010).
6. A. J. L. Adam, "Review of near-field terahertz measurement methods and their applications," J. Infrared Milli. Terahz. Waves **32**, 976–1019 (2011).
7. P. C. M. Planken, C. E. W. M. van Rijmenam, and R. N. Schouten, "Opto-electronic pulsed THz systems," Semicon. Sci. Techn. **20**, s121–s127 (2005).
8. A. J. Huber, F. Keilmann, J. Wittborn, J. Aizpurua, and R. Hillenbrand, "Terahertz near-field nanoscopy of mobile carriers in single semiconductor nanodevices," Nano Lett. **8**, 3766–3770 (2008).
9. H. -T. Chen, R. Kersting, and G. C. Cho, "Terahertz imaging with nanometer resolution," Appl. Phys. Lett. **83**, 3009–3011 (2003).
10. A. Bitzer and M. Walther, "Terahertz near-field imaging of metallic sub-wavelength holes and hole arrays," Appl. Phys. Lett. **92**, 231101 (2008).

#178642 - $15.00 USD Received 24 Oct 2012; revised 30 Dec 2012; accepted 31 Dec 2012; published 10 Jan 2013

11. A. Bitzer, H. Merbold, A. Thoman, T. Feurer, H. Helm, and M. Walther, "Terahertz near-field imaging of electric and magnetic resonances of a planar metamaterial," Opt. Express **17**, 3826–3834 (2009).
12. M. Wächter, M. Nagel, and H. Kurz, "Tapered photoconductive field probe with subwavelength spatial resolution", Appl. Phys. Lett. **95**, 041112 (2009).
13. M. Nagel, A. Michalski, T. Botzem, and H. Kurz, "Near-field investigation of THz surface-wave emission from optically excited graphite flakes," Opt. Express **19**, 4667–4672 (2011).
14. M. A. Seo, A. J. L. Adam, J. H. Kang, J. W. Lee, S. C. Jeoung, Q. H. Park, P. C. M. Planken, and D. S. Kim, "Fourier-transform terahertz near-field imaging of one-dimensional slit arrays: mapping of electric-field-, magnetic-field-, and Poynting vectors," Opt. Express **15**, 11781–11789 (2007).
15. A. J. L. Adam, J. M. Brok, M. A. Seo, K. J. Ahn, D. S. Kim, J. H. Kang, Q. H. Park, M. Nagel, and P. C. M. Planken, "Advanced terahertz electric near-field measurements at sub-wavelength diameter metallic apertures," Opt. Express **16**, 7407–7417 (2008).
16. J. R. Knab, A. J. L. Adam, M. Nagel, E. Shaner, M. A. Seo, D. S. Kim, and P. C. M. Planken, "Terahertz near-Field vectorial imaging of subwavelength apertures and aperture arrays," Opt. Express **17**, 15072–15086 (2009).
17. N. Kumar, A. C. Strikwerda, K. Fan, X. Zhang, R. D. Averitt, P. C. M. Planken, and A. J. L. Adam," THz near-field Faraday imaging in hybrid metamaterials," Opt. Express **20**, 11277–11287 (2012).
18. J. R. Knab, A. J. L. Adam, R. Chakkittakandy, and P. C. M. Planken, "Terahertz near-field microspectroscopy," Appl. Phys. Lett. **97**, 031115 (2010).
19. L. Guestin, A. J. L. Adam, J. R. Knab, M. Nagel, and P. C. M. Planken, "Influence of the dielectric substrate on the terahertz electric near-field of a hole in a metal," Opt. Express **17**, 17412–17425 (2009).
20. Y. Rong and K. A. Zaki, "Characteristics of generalized rectangular and circular ridge waveguides," IEEE Trans. Microwave Theory Tech. **48**, 258–265 (2000).
21. A. Agrawal, H. Cao, and A. Nahata, "Time-domain analysis of enhanced transmission through a single subwavelength aperture," Opt. Express **13**, 3535–3542 (2005).
22. G. Zhao, R. N. Schouten, N. van der Valk, W. Th. Wenckebach, and P. C. M. Planken, "Design and performance of a THz emission and detection setup based on a semi-insulating GaAs emitter," Rev. Sci. Instrum. **73**, 1715–1719 (2002).
23. O. Mitrofanov, M. Lee, J. W. P. Hsu, L. N. Pfeiffer, K. W. West, J. D. Wynn, and J. F. Federici, "Terahertz pulse propagation through small apertures," Appl. Phys. Lett. **79**, 907–909 (2001).
24. O. Mitrofanov, R. Harel, M. Lee, L. N. Pfeiffer, K. W. West, J. D. Wynn, and J. Federici, "Study of single-cycle pulse propagation inside a terahertz near-field probe," Appl. Phys. Lett. **78**, 252–254 (2001).
25. O. Mitrofanov, M. Lee, J. W. P. Hsu, R. Harel, J. F. Federici, J. D. Wynn, L. N. Pfeiffer, and K. W. West, "Collection-mode near-field imaging With 0.5-THz Pulses," IEEE J. Sel. Top. Quant. Electron.**7**, 600–607 (2001).
26. R. Chakkittakandy, A. W. M. Corver, and P. C. M. Planken, "Quasi-near field terahertz generation and detection," Opt. Express **16**, 12794–12805 (2008).
27. M. Yamaguchi, F. Miyamaru, K. Yamamoto, M. Tani, and M. Hangyo, "Terahertz absorption spectra of L-, D-, and DL-alanine and their application to determination of enantiometric composition," Appl. Phys. Lett. **86**, 053903 (2005).
28. E. R. Brown, J. E. Bjarnason, A. M. Fedor, and T. M. Korter,"On the strong and narrow absorption feature in lactose at 0.53 THz," Appl. Phys. Lett. **90**, 061908 (2007).
29. C. J. Bouwkamp, "On Bethe's theory of diffraction by small holes," Philips Res. Rep. **5**, 321–332 (1950).
30. C. J. Bouwkamp, "On the diffraction of electromagnetic waves by small circular disks and holes," Philips Res. Rep. **5**, 401–422 (1950).

1. Introduction

Terahertz (THz) spectroscopy is a powerful tool for the identification of inorganic crystals and organic molecular crystals through their phonon absorption spectra. [1–5] One of the problems with standard THz spectroscopy, however, is that diffraction limits the size of the smallest samples for which a spectrum can be measured, to values of a few hundred micrometers or more. When a crystal is much smaller than this, light simply diffracts around it and in the far-field, little or no information about the crystal can be extracted from the measured THz electric field. One way to overcome this problem is by performing near-field measurements. When the THz electric field is measured in a small volume of space around an object, the frequency-dependent dielectric function of that object can, in principle, be extracted from such a measurement, irrespective of the object's size. In the past, several methods have been used to measure the near-field of objects. [6] These include THz apertureless near-field scanning optical microscopy [7–9], which uses a small metal tip to sample the THz light in a small, sub-

#178642 - $15.00 USD Received 24 Oct 2012; revised 30 Dec 2012; accepted 31 Dec 2012; published 10 Jan 2013

wavelength sized volume, as well as THz photoconductive sampling using antennas [10–13], electro-optic detection with a tightly focused probe beam [14–16] and, most recently, magneto-optic sampling of a metamaterial [17]. In near-field measurements, it is important to suppress unwanted background THz light coming from the incident THz electric field or from light scattered off objects elsewhere. This often requires modulation techniques that add complexity to an already complicated near-field setup. An example is a typical THz ANSOM experiment in which the tip-sample distance is modulated with subsequent detection of the THz light at a harmonic of the modulation frequency. [8] A simple method to eliminate the background in near-field spectroscopy is to send light through tiny, sample-filled waveguides in metal foils. Loosely speaking, confining the light to the sample-filled waveguide means that all the THz light that reaches the other side of the waveguide must have interacted with the sample, thus eliminating other contributions to the measured THz field. [18] This techniques works very well for circular waveguides as small as approximately half-a-wavelength in diameter, but not for smaller ones. The reason for this is that circular waveguides have a cut-off frequency below which almost no light can reach the end of the waveguide. [19] When the diameter of the waveguide decreases, the cut-off frequency shifts to higher frequencies and absorption by samples at frequencies below the cut-off frequency can no longer be measured. In the range of 0.2 to 3 THz, this means that waveguides smaller than about 150 μm diameter cannot not be used. It is, however, possible to increase the transmission through waveguides by structuring the aperture itself, although this makes fabrication of the resulting waveguides more complex. [20] Alternatively, one can create, for example, a bulls-eye structure surrounding the aperture which increases the aperture transmission, albeit in a narrower bandwidth. [21]

Here we show how one can measure THz absorption lines of crystalline samples as small as 10 μm in diameter, using ultrashort "waveguides" formed by creating simple, circular apertures in thin metal films on a substrate. This method is based on the property that, in contrast to long cylindrical waveguides, apertures in *thin* films lack a well-defined cut-off frequency and thus show significant transmission in the near-field far below the cut-off frequency of a "regular" waveguide of the same diameter. [15, 19] We measure the THz electric field on the shadow side of these apertures, on which tiny crystals of cesium iodide (CsI) are deposited, using near-field electro-optic sampling. Surprisingly, we find that the measured absorption line shape of the 1.8 THz CsI phonon resonance mirrors both the frequency-dependent, refractive-index profile of the phonon resonance and the bulk phonon absorption line shape. This is supported by calculations of the electric near-field behind these apertures, which demonstrate that the amplitude transmission of these filled apertures is not only a function of the phonon absorption, but also a strong function of the frequency-dependent, refractive index of the filling material. Our technique has allowed us to measure absorption spectra of sample volumes as small as $\sim 5\times 10^{-16}$ m^3, corresponding to 0.5 pl.

2. Experimental setup

Part of the experimental setup used to measure the near-field behind the filled apertures is shown in Fig. 1. Small apertures of 10, 20, and 40 μm diameter are defined in a 500 nm-thick gold film, directly deposited on a 500 μm-thick, (111) oriented GaP electro-optic crystal. [15] The apertures are covered with CsI crystals formed via evaporation of a tiny drop of a CsI solution, which was deposited on the aperture using a microinjection system (PLI-100 Plus Pico-Injector, from Harvard Apparatus). If the resulting crystal was much larger than the aperture, parts of the crystal were mechanically removed until a crystal size was obtained which was not much larger than the in-plane size of the aperture. An example of a CsI crystal thus deposited on a 20 μm diameter aperture is shown in Fig. 1. The aperture is illuminated with THz pulses that are generated in a photoconductive switch with 20 fs laser pulses from a laser

#178642 - $15.00 USD Received 24 Oct 2012; revised 30 Dec 2012; accepted 31 Dec 2012; published 10 Jan 2013

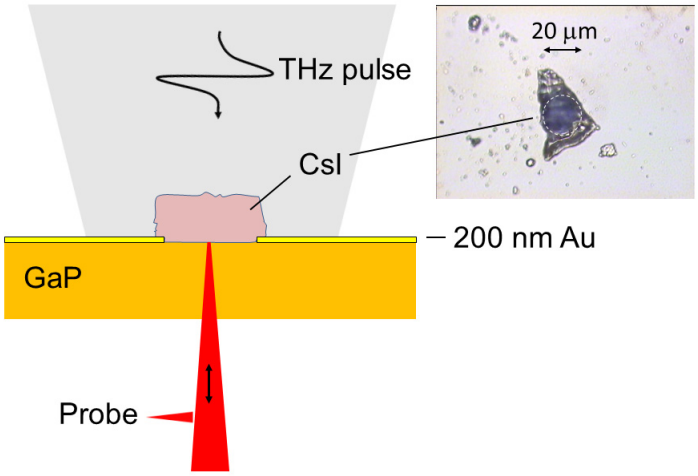

Fig. 1. (a) Schematic drawing of part of the experimental setup. A 500 nm-thick gold film with a lithographically fabricated aperture is deposited onto a (111) oriented GaP electro-optic crystal. From above, a THz pulse is focused onto the aperture. From below, femtosecond probe laser pulses are focused onto the front surface to an approximately 5 μm diameter spot size. The probe pulses sample the THz electric near-field immediately behind the aperture. On the right is a photograph of a CsI crystal deposited onto a 20 μm diameter aperture, taken with a conventional optical microscope.

oscillator (Femtolasers) operating at a central wavelength of around 800 nm. [22] From below, a synchronized, linearly polarized probe laser pulse is tightly focused to a $\sim$5μm diameter spot immediately below the center of the aperture in the gold film. The transverse component of the THz electric near-field of the aperture elliptically polarizes the probe pulse, which reflects from the GaP surface towards a standard differential detection setup. This setup measures the probe pulse ellipticity, which is proportional to a single, instantaneous, THz electric-field value, as a function of the time delay between the incident THz pulse and the probe pulse. In this way, a 20 ps long THz electric-field transient is obtained in a stroboscopic manner. To reduce absorption of THz radiation by water vapor, the entire setup is enclosed in a box that is purged with dry nitrogen gas. CsI was chosen as the sample material because it has a fairly sharp and strong phonon resonance at 1.8 THz. [1]

3. Results and discussion

An example of a measurement of the incident THz electric field as a function of time, obtained using a bare part of the same (111) oriented GaP crystal on which the CsI samples were deposited, is shown in Fig. 2(a). Figure 2(a) shows that the incident electric field consists of nearly a single cycle. In Fig. 2(b) we show the THz electric field as a function of time, measured behind the smallest aperture (10 μm diameter). The electric field consists of a sharp spike with a full width at half maximum (FWHM) of a few hundred femtoseconds only, which is considerably less than the FWHM of the peaks of the incident field. This can only be explained by the fact that the THz field transmitted by the aperture is dominated by higher frequencies than the

#178642 - $15.00 USD Received 24 Oct 2012; revised 30 Dec 2012; accepted 31 Dec 2012; published 10 Jan 2013

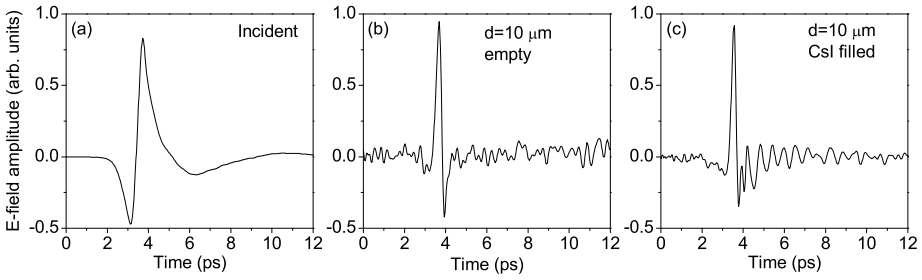

Fig. 2. (a) Measured electric field as a function of time of the THz pulse incident on the aperture. (b) Electric near-field as a function of time measured behind an unfilled 10 μm aperture. (c) Electric near-field as a function of time measured behind a 10 μm aperture covered with a small CsI crystal.

field incident on the sample. As observed in previous works [15, 18, 23–25], this is because the aperture functions like a high-pass filter, predominantly transmitting the higher THz frequencies. As a result of this, the peak field amplitude measured behind the aperture is approximately 250 times weaker than the measured peak amplitude of the incident THz field.

In Fig. 2(c) we plot the THz electric field as a function of time, measured behind the same 10 μm diameter aperture, which is now covered with CsI. The electric field consists of a sharp spike followed by an oscillatory, decaying signal having a period of about 0.57 ps, corresponding to a frequency of 1.75 THz. It is perhaps surprising that the frequency of the oscillatory signal does not simply correspond to the 1.8 THz TO-phonon frequency of CsI, but is somewhat lower. Results for the 20 μm and 40 μm apertures look similar (not shown here), although the amplitude of the measured electric near-field increases for increasing aperture size. A direct comparison of the amplitudes transmitted by the different CsI-filled apertures is not possible here, since the sizes and thicknesses of the CsI crystals covering the apertures, vary and are not known precisely.

The normalized spectra of the THz electric near-fields measured behind the empty and behind the CsI-filled apertures can easily be obtained by Fast-Fourier transforming the measured signals. The results for aperture diameters of 10, 20 and 40 μm are shown in Figs. 3(a)-3(c) and 3(d)-3(f) respectively. For each measurement, the data were normalized to the spectrum of the incident THz field. The spectral amplitude measured behind the empty apertures increases as a function of frequency, similar to previous measurements for larger diameter apertures. [15] The quasi-periodic oscillations seen at higher frequencies for the 10 μm diameter aperture in Fig. 3(a) are the result of the noise seen in the time-domain signal in Fig. 2(b). They are not reproducible. All spectra obtained for the filled apertures show a peak at approximately 1.7 THz and a dip around 1.8 THz. The spectra are thus different from the simple absorption dips observed in the THz spectra of pressed pellets of organic crystals [5, 26–28], or in the near-field spectra of filled waveguides [18]. The increase in the transmission around 1.7 THz is noteworthy, especially for the 10 and 20 μm diameter apertures. For the 40 μm diameter aperture, this feature appears less pronounced. The increases of the aperture transmission with frequency for the smallest apertures is faster than would be expected from the well-understood *slow* increase in the transmission of a sub-wavelength sized aperture when the frequency increases from lower

#178642 - $15.00 USD Received 24 Oct 2012; revised 30 Dec 2012; accepted 31 Dec 2012; published 10 Jan 2013

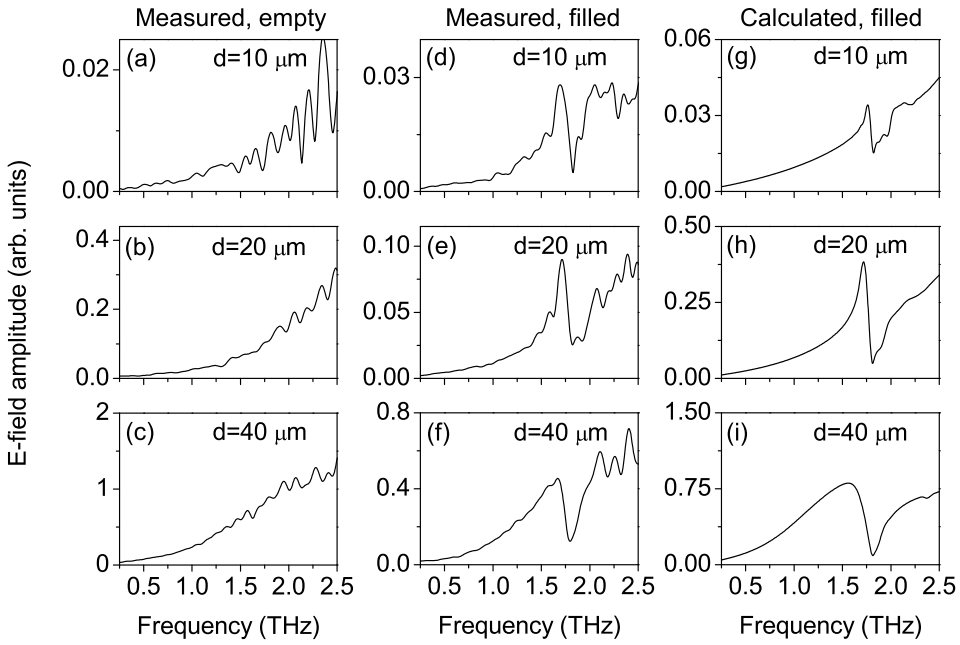

Fig. 3. (a)-(c) Electric near-field amplitude as a function of frequency, measured behind empty apertures of 10, 20 and 40 μm diameter. (d)-(f) Electric near-field amplitude as a function of frequency, measured behind apertures of 10, 20 and 40 μm diameter, filled with CsI. For each of the measurements, the data were normalized with respect to the spectrum of the incident THz pulse, obtained using a bare part of the same (111) oriented GaP crystal on which the CsI samples were deposited.(g)-(i) Electric near-field amplitude as a function of frequency, calculated behind apertures of 10, 20, and 40 μm diameter, filled with CsI.

to higher values. [15] The apparent irregular variations in the spectral amplitude for frequencies above approximately 2 THz in Figs. 3(a)-3(f) are not reproducible. They arise from a decrease in the emitted power of our biased GaAs emitter at higher frequencies, and thus gives rise to more noise in the data shown in Fig. 3. For the smallest aperture (10 μm diameter), the noise in the measured electric near-field is also large at lower frequencies, simply because the electric field behind such a small aperture is very weak and thus difficult to measure.

To confirm that our results are not due to a measurement artifact, we have also performed full numerical simulations of the THz electric near-field behind the apertures using a commercial software package (CST Microwave Studio). The refractive index of GaP is taken to be 3.3. These calculations use the frequency-dependent, complex dielectric constant of CsI near the phonon resonance, which is given by:

$$\varepsilon(\omega) = \varepsilon_\infty + (\varepsilon_{stat} - \varepsilon_\infty)\frac{\omega_{TO}^2}{(\omega_{TO}^2 - \omega^2 - i\omega\Gamma_{TO})} \quad (1)$$

where ε_∞ is the electronic dielectric constant, ε_{stat} is the static dielectric constant, ω_{TO} is the angular transverse optical phonon frequency, and Γ_{TO} the transverse optical

#178642 - $15.00 USD Received 24 Oct 2012; revised 30 Dec 2012; accepted 31 Dec 2012; published 10 Jan 2013

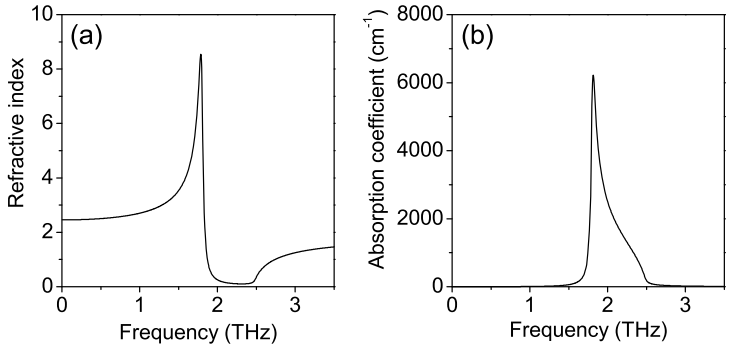

Fig. 4. (a) Refractive index, n, and (b) absorption coefficient, α, as a function of frequency, calculated using Eq. (1), with parameters adapted from ref. [1]. We have used ω_{TO} =$2\pi\times1.8\times10^{12}$ rad/s, Γ_{TO} =0.3×10^{12} rad/s, ε_∞ =3.17, and ε_{stat} =6.03.

phonon angular damping frequency. For the simulations, we used the following values: ω_{TO} =$2\pi\times1.8\times10^{12}$ rad/s, Γ_{TO} =0.3×10^{12} rad/s, ε_∞ =3.17, and ε_{stat} =6.03. These values were chosen because they give the best agreement between the measurements and the calculations. As such, they differ slightly from those reported in reference [1].

From Eq. (1) we obtain the complex refractive index $\tilde{n}(\omega)=\sqrt{\varepsilon(\omega)}$. With $\Re$ and $\Im$ denoting the real and imaginary part respectively, we write for the real part of the refractive index $n(\omega)=\Re(\tilde{n}(\omega))$, and for the absorption coefficient $\alpha(\omega)=2\omega\Im(\tilde{n}(\omega))/c$. In Fig. 4(a) we plot the real part of the refractive index, $n(\omega)$, and in Fig. 4(b) the absorption coefficient, $\alpha(\omega)$, calculated using the parameters mentioned above.

In all calculations of the electric near-field, we assume that the CsI crystal has a thickness of 5 μm and that it uniformly fills the apertures, but does not cover the gold surrounding the aperture. The results of the calculations of the electric near-field in-plane component, E_x, 10 μm below the apertures, are shown in Figs. 3(g)-3(i). The calculations are in excellent agreement with the measurements. For increasing frequencies, the electric near-field first reaches a maximum around 1.7 THz followed by a dip around 1.8 THz. As in the experiments, the peak in the calculated electric near-field, around a frequency of 1.7 THz, is less pronounced for the largest aperture used. The results provide further evidence that our measurement technique indeed measures the near-field of the CsI filled apertures. If we can assume a CsI layer thickness of 5 μm, having transverse dimensions of 10 μm by 10 μm, which just covers the smallest aperture diameter, we calculate a sample volume of about 5×10^{-16} m^3, equivalent to 0.5 pl, for which we have measured the THz absorption/refractive index spectrum.

A comparison between Fig. 3 and Fig. 4 shows that around the CsI TO-phonon resonance, the measured electric near-field amplitude as a function of frequency, is not simply explained by the calculated absorption coefficient as a function of frequency, plotted in Fig. 4(b). In fact, the measured line shape also has some semblance to the dispersive *refractive-index* line shape shown in Fig. 4(a). Insight into why this is the case can be obtained by taking a closer look at the analytical expression for the electric near-field behind a sub-wavelength diameter aperture calculated by Bouwkamp. [29, 30] The Bouwkamp model assumes that the metal is a perfect conductor and that it is infinitely thin. The x-component of the electric field amplitude behind

#178642 - $15.00 USD Received 24 Oct 2012; revised 30 Dec 2012; accepted 31 Dec 2012; published 10 Jan 2013

the aperture is given by:

$$E_x(x,y,z) = E_0\left[ikz - \frac{2}{\pi}ikau\left(1 + v\arctan(v) + \frac{1}{3}\frac{1}{u^2+v^2} + \frac{x^2-y^2}{3a^2(u^2+v^2)(1+v^2)^2}\right)\right] \quad (2)$$

where

$$u^2 = \frac{1}{2}\left[1 - \frac{x^2+y^2+z^2}{a^2}\right] + \frac{1}{2}\sqrt{\left[\frac{x^2+y^2+z^2}{a^2} - 1\right]^2 + \frac{4z^2}{a^2}} \quad (3)$$

and

$$v^2 = \frac{z^2}{a^2u^2}. \quad (4)$$

E_0 is the incident field amplitude, k is the wave number, $a = d/2$ is the radius of the aperture, with $ka = 2\pi a/\lambda \ll 1$, x and y are the Cartesian coordinates in the plane of the conductor, z is the Cartesian coordinate equivalent to the distance behind the aperture, and ϕ is the azimuthal angle. The point $(x = 0, y = 0, z = 0)$ corresponds to the center of the aperture. Strictly speaking, Eq. (2) is not valid for our system since it assumes that the entire space above and below the aperture is filled with the same material. In the experiment, the space behind the aperture is partly filled with GaP, and above it is partly filled with CsI. Keeping this limitation in mind, Eq. (2) shows that the electric field immediately behind the aperture is proportional to the wavenumber, k. This contrasts with the usual expression for a plane wave propagating in matter in the z-direction, where k usually only appears in the e^{ikz} exponent. k can be written as: $k = \omega\tilde{n}/c$, where $\tilde{n}$ is the complex refractive index. This not only describes the absorption of a material, but also the dispersion, which is present in the real refractive index as a function of frequency. Here, the frequency-dependent electric near-field behind the aperture is proportional to the real refractive index profile of the CsI phonon resonance. For weak THz resonances, typically observed in organic crystals having absorption coefficients of tens to hundreds of wavenumbers, this effect is mostly very weak. For the strong phonon resonance of a crystal such as CsI, the effect is rather pronounced. One further thing to note is that Eq. (2) shows that there should be no dependence of the shape of the transmitted spectrum on the exact location (x,y,z) below the aperture where the field is observed. The effect of changing x and y by moving closer to the aperture edge is to reduce the amplitude of all frequencies equally. Directly under the metal, next to the aperture, the measured E_x was too small to measure.

An intuitive explanation for why the transmission of the apertures increases around 1.7 THz can be found by first considering a true waveguide: when a waveguide is filled with a dielectric, the cut-off frequency shifts to lower frequencies. [19] This is because the wavelength in a dielectric material is shorter than the vacuum wavelength, giving rise to an increase in the transmission at lower frequencies. Here, the apertures in the metal film cannot be considered true waveguides and as such do not have a clearly defined cut-off frequency. Nevertheless, they do show a frequency-dependent transmission and when filled with a dielectric material, this transmission spectrum is, loosely speaking, scaled towards lower frequencies. [18, 19] In the case of CsI, the refractive index strongly varies around the transverse-optic phonon resonance, peaking slightly below the resonance frequency. Starting from a frequency below the resonance frequency, the aperture therefore behaves like a dielectric filled aperture with a high refractive index material, initially causing the transmission to become larger. When the frequency increases and approaches the resonance frequency, the absorption becomes stronger, finally leading to a decrease in the transmission. These two competing effects give rise to a maximum transmission which peaks around 1.7 THz.

It is remarkable that measurable signals are obtained for apertures with diameters as small as 10 μm. Part of the explanation for this is that we measure in the near-field of the apertures

#178642 - $15.00 USD Received 24 Oct 2012; revised 30 Dec 2012; accepted 31 Dec 2012; published 10 Jan 2013

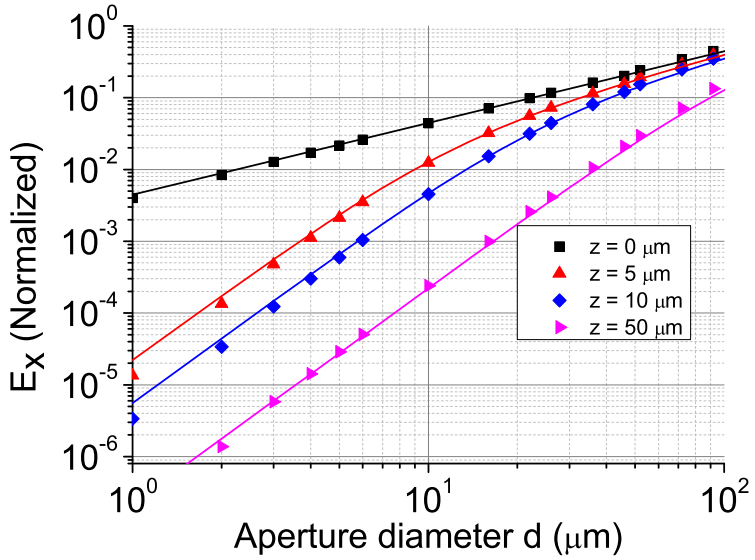

Fig. 5. Normalized electric near-field as a function of aperture diameter, calculated for four different distances, z, behind the center of the aperture: z =0, 5, 10, 50 μm. The data points represent numerical calculations at a frequency of 0.5 THz using CST Microwave Studio. The solid lines are calculated using Eq. (2).

where signals are relatively strong. This is illustrated in Fig. 5, where we plot the calculated in-plane electric field component, E_x, behind an aperture in free space as a function of aperture diameter, for four different distances behind the aperture: 0, 5, 10, and 50 μm. The solid lines are calculated using Eq. (2), whereas the points correspond to the numerical calculations, performed for a frequency of 0.5 THz. Figure 5 shows that when the distance to an aperture is on the order of the radius of the aperture or larger, the field strength decreases with the third power of the aperture diameter. Closer to the aperture, however, the dependence is much weaker and becomes linear in the plane of the aperture. This near-field region, defined here as a spherical volume of space around the aperture having a radius roughly similar to the aperture radius, is therefore a suitable region in which to perform spectroscopy. The signals are relatively strong and show a weaker dependence on the aperture diameter than the far-field signals. We would like to point out that the analytical and numerical calculations show good agreement. The calculations clearly show that it is advantageous to measure the near-field close to the apertures where signals are relatively strong. Based on this, and on the relatively strong measured signals shown in Fig. 3, we can conclude that smaller apertures and thus smaller sample volumes may be used in the future, even though depositing and positioning samples with smaller sizes on apertures smaller than 10μm in diameter will be more challenging. There is a distinct advantage to measuring the fairly small THz electric field behind a small aperture, rather than measuring the electric field of a CsI crystal in the far-field. In the far-field, without the use of an aperture, the strong THz signal would hardly show any evidence of the presence of the CsI crystal, since the CsI crystal is much smaller than the wavelength and the THz light would simply diffract around the crystal. Observing the CsI resonance in this case boils down to measuring

#178642 - $15.00 USD Received 24 Oct 2012; revised 30 Dec 2012; accepted 31 Dec 2012; published 10 Jan 2013

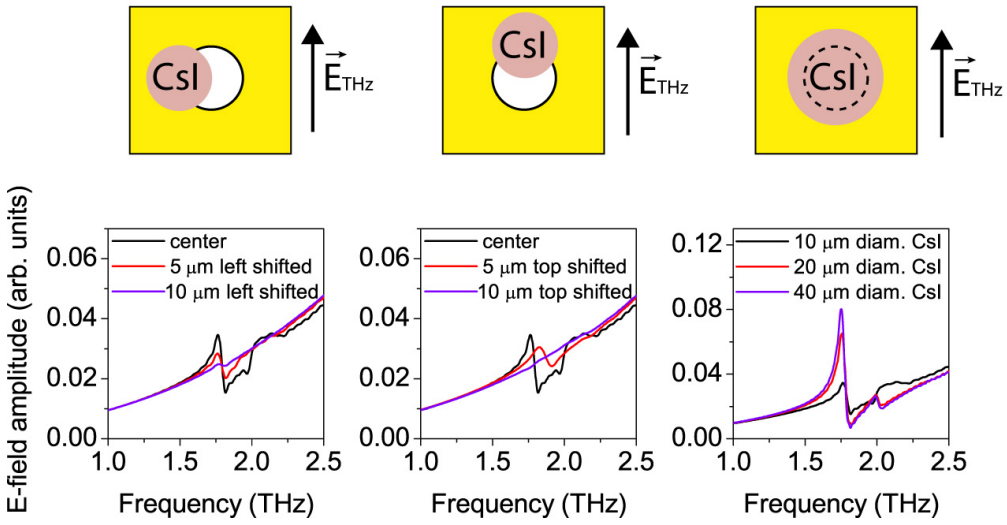

Fig. 6. (a) Normalized electric near-field behind a 10 μm diameter aperture, calculated for three different positions of a 10 μm diameter, 5 μm thick CsI crystal placed on top of the aperture. The three positions correspond to a crystal centered at the aperture, and shifted 5 and 10 μm to the left, respectively. The illustration above the graph shows the polarization direction of the incident field and a CsI sample displaced to the left of the center of the aperture in the gold film. (b) Normalized electric near-field behind a 10 μm diameter aperture, calculated for three different positions of a 10 μm diameter, 5 μm thick CsI crystal. The three positions correspond to a crystal centered at the aperture, and shifted 5 and 10 μm upwards, respectively. (c) Normalized electric near-field behind a 10 μm diameter aperture, calculated for three different crystal diameters of 10, 20 and 40 μm respectively. The crystal thickness is 5 μm. As in Figs. 3(g)-3(i), the fields are calculated in the center of the aperture, 10 μm below the surface of the GaP crystal.

a very small *change* in the THz electric field over a large background signal. This requires an extremely stable THz signal which is equivalent to a good signal-to-noise (S/N) ratio in the measurements. In the case of a CsI crystal on top of an aperture, all the light transmitted by the aperture, although small in amplitude, has interacted with the CsI. The ability to observe the CsI resonance in this case only depends on the ability of the setup to measure small *absolute* signals. This property is more related to the dynamic range of the system and puts less stringent demands on the S/N of the system. [7, 22]

For practical applications, it is important to know the effect on the transmitted signals when the crystals only partially cover the aperture, or when the crystal sizes are much larger than the aperture diameter. We have therefore also numerically calculated the spectra transmitted by the smallest, 10 μm diameter, CsI covered aperture taking these non-ideal circumstances into account. In Fig. 6(a) we plot the calculated normalized spectra transmitted by the 10 μm diameter aperture for three locations of a cylindrical, 5 μm thick, 10 μm diameter CsI crystal: centered on the aperture and filling it, shifted by 5 μm in a direction perpendicular to the polarization direction of the incident field ("left-shifted"), and also shifted by 10 μm in the same direction. In the "left shifted" case and in the "top shifted" case discussed below, we assume that inside the aperture, the CsI doesn't touch the GaP, leaving a 0.5 μm gap between the CsI and the GaP. The figure clearly demonstrates that the phonon signature present in the transmitted spectra becomes less pronounced as the crystal is shifted by 5 μm, and almost disappears when

#178642 - $15.00 USD Received 24 Oct 2012; revised 30 Dec 2012; accepted 31 Dec 2012; published 10 Jan 2013

the crystal is exactly at the edge of the hole, which corresponds to the 10 μm, "left-shifted" case. In Fig. 6(b) we plot the calculated normalized transmission spectra for the case when the 10 μm diameter CsI crystal is moved in a direction along the polarization direction of the incident THz electric field ("top-shifted"). For comparison, the spectrum calculated when the crystal is centered on the aperture is also shown. When the crystal is shifted 5 μm, the calculated spectrum looks different compared to the spectra shown in Fig. 6(a). Most notable is the fact that the dispersive-like feature seems to have shifted slightly to higher frequencies and looks different in shape. The same is true for the spectrum calculated for the 10 μm shifted case but here the phonon signature is much weaker. The reason why the spectra in Fig. 6(a) and (b) look different is that the two cases correspond to two different excitation geometries. For the calculation of the curves in Fig. 6(b), in the center of the aperture, the incident field is polarized in a direction perpendicular to the edge of the crystal. In this case, the diffracted field is spatially more modified ("diffracted") by the edge than in the case that the field is polarized more or less parallel to the edge. Note that in neither case is the field perpendicular or parallel *everywhere* to the edge of the crystal, which is circularly shaped. Edge diffraction is as much the result of the geometry of the sample as of the frequency-dependent complex dielectric function of the material. The combination of the two determines the ultimate shape of the transmitted field in this case. A detailed analysis of the effects of edge diffraction on the transmission of partially covered apertures, however, is beyond the scope of this work. Nonetheless, one important conclusion that can be drawn from these results is that samples located a small distance from the aperture edge will have little or no effect on the transmitted spectra.

It is also interesting to study the effect of CsI sample size on the spectra transmitted by the aperture. In Fig. 6(c) we plot the normalized transmission spectrum of a 10 μm diameter aperture covered with a 10 μm diameter CsI crystal, a 20 μm diameter crystal and a 40 μm diameter crystal. The figure clearly shows that larger crystals lead to significantly stronger signals. The change is largest when going from a 10 μm diameter crystal to a 20 μm diameter crystal where, at about 1.75 THz, we observe that the transmission increases by a factor of about two. For the 40 μm diameter crystal, the maximum transmitted field at a frequency of about 1.75 THz is about 2.3 larger times larger than for the 10 μm diameter aperture. The increase in the transmission for increasing crystal size is, in fact, something we have observed in our measurements also (not shown here). A larger crystal apparently funnels more energy through the hole at certain frequencies than a smaller one, but for even larger samples, further increases are small.

Finally, we can speculate on the ability of the technique to measure resonances of other systems than CsI. Many molecular crystals have phonon resonances in the THz domain. [1–5] The ability to measure small quantities of these materials will depend on the strength of the absorption lines and on the value of the corresponding refractive-index. For an absorption coefficient of $\sim$500 cm^{-1}, an order-of-magnitude estimate for many molecular crystal resonances in the THz domain, a layer of tens of microns thickness may be required to obtain a measurable effect on the absorption. In view of the sample-size dependence discussed above, the signal may be enhanced further by using crystals that are twice as large as the aperture diameter. For stronger resonances, such as those typically observed at higher THz frequencies, smaller quantities are allowed. Our technique may therefore be able to greatly reduce the amount of material required for the identification of molecular crystals.

4. Conclusions

We have measured terahertz near-field spectra of microscopic CsI crystals, deposited on individual sub-wavelength-sized apertures as small as 10 μm in diameter, created in thin gold films

#178642 - $15.00 USD Received 24 Oct 2012; revised 30 Dec 2012; accepted 31 Dec 2012; published 10 Jan 2013

on a substrate. Our results show that the spectra observed immediately behind the apertures can be understood as resulting from the competition between an increase in the aperture transmission due to an increasing refractive index, and a decrease caused by increasing absorption around the TO-phonon resonance of CsI. Our aperture method is background-free, and can be used to identify small quantities of crystals. A careful comparison with numerical simulations allows us to extract the frequency-dependent refractive index and absorption. The experimental results are in very good agreement with these numerical calculations and we predict that measurements of smaller samples deposited on apertures smaller than 10 μm may be possible.

Acknowledgments

PCMP and AJLA gratefully acknowledge financial support from the Nederlandse Organisatie voor Wetenschappelijk Onderzoek NWO for a VICI grant and VENI grant respectively. This work was performed, in part, at the Center for Integrated Nanotechnologies, a U.S. Department of Energy, Office of Basic Energy Sciences user facility. Sandia National Laboratories is a multi-program laboratory managed and operated by Sandia Corporation, a wholly owned subsidiary of Lockheed Martin Corporation, for the U.S. Department of Energy's National Nuclear Security Administration under contract DE-AC04-94AL85000.

#178642 - $15.00 USD Received 24 Oct 2012; revised 30 Dec 2012; accepted 31 Dec 2012; published 10 Jan 2013